IEEE Access
Multidisciplinary | Rapid Review | Open Access Journal

Received September 30, 2017, accepted October 27, 2017, date of publication November 8, 2017, date of current version December 5, 2017.

Digital Object Identifier 10.1109/ACCESS.2017.2771200

Practical Implementation of Index Modulation-Based Waveforms

SELAHATTIN GOKCELI[1], (Student Member, IEEE), ERTUGRUL BASAR[1], (Senior Member, IEEE), MIAOWEN WEN[2], (Member, IEEE), AND GUNES KARABULUT KURT[1], (Senior Member, IEEE)

[1]Department of Communications and Electronics Engineering, Istanbul Technical University, 34469 Istanbul, Turkey
[2]School of Electronic and Information Engineering, South China University of Technology, Guangzhou 510640, China

Corresponding author: Selahattin Gokceli (gokcelis@itu.edu.tr)

ABSTRACT Orthogonal frequency division multiplexing (OFDM) with index modulation (OFDM-IM) technique has been recently proposed to provide performance improvements over conventional OFDM. OFDM-IM includes a different data transmission mechanism, where additional data bits are transmitted over subcarrier patterns by specifically activating selected subcarriers and nulling the others. However, such a mechanism inherently causes some inefficiency due to the inactive subcarriers. To improve the spectral efficiency of the OFDM-IM technique, dual-mode OFDM with index modulation (DM-OFDM) is proposed, where nulled subcarriers are activated by using a second signal constellation. With DM-OFDM, a significant data rate improvement can be obtained. As an important missing issue in the literature, OFDM-IM and its effective variations, such as DM-OFDM, have only been studied in terms of computer simulations and theoretical analysis. Therefore, their real-time performance is not yet investigated to assess their potential for next-generation networks. Addressing this gap, in this paper, OFDM-IM and DM-OFDM techniques are implemented in real-time by using software defined radio technology. National Instruments USRP-2921 nodes are used in a single-input single-output configuration. With this implementation, detailed real-time results and performance observations are provided. Moreover, a hybrid OFDM-IM (H-OFDM-IM) scheme, which can be seen as the combination of OFDM-IM and DM-OFDM, is proposed by targeting the limitations of both OFDM-IM and DM-OFDM in terms of spectral containment and error performance. With H-OFDM-IM, noticeable improvements in spectral containment and error performance can be obtained, and these observations show its suitability for real-time use and next-generation networks. With comprehensive computer simulation and test results, these claims are verified.

INDEX TERMS Index modulation, OFDM, DM-OFDM, software defined radio, waveform.

I. INTRODUCTION

The number of wireless users continues to increase rapidly and the management of frequency resources becomes more difficult to handle day by day. This fact even affects current wireless technologies and the expected service quality levels cannot be met in some circumstances. In accordance with this, research activities target new signal processing techniques in the communications field. Particularly in 5G research activities, some novel physical layer techniques are proposed to improve the limitations of traditional techniques. As an important component of the wireless transmission structure, the utilized waveform plays a key role in transmission process, determining the corresponding performance characteristics. In recent years, orthogonal frequency division multiplexing (OFDM) technique has been the dominant waveform choice in various wireless technologies. Main advantages of OFDM are its robustness to frequency-selective fading and its simple implementation. However, OFDM has some major drawbacks that would threaten its popularity in next-generation wireless technologies, especially in 5G wireless networks [1].

The main drawbacks of OFDM are the use of cyclic prefix (CP), which decreases the spectral efficiency, the rectangular shape filter that brings high sidelobe attenuation, the peak-to-average power ratio (PAPR) problem that brings important power consumption costs to mobile devices and its high sensitivity to carrier frequency offset (CFO). These problems cause noticeable error performance loss and

spectral efficiency reduction. In order to overcome these problems, some new methodologies have been proposed in the literature. One important waveform candidate that provides remarkable improvements over OFDM is the OFDM with index modulation (OFDM-IM) technique, which is proposed in [2]. Similar to the principle of spatial modulation OFDM (SM-OFDM), where in addition to the ordinary in-phase and quadrature modulation, data bits are also transmitted with the selection of active antennas [3], [4], OFDM-IM performs the transmission of data bits with specific active subcarrier patterns through IM. Therefore, in OFDM-IM, some subcarriers are nulled to represent the corresponding active subcarrier pattern. Such a procedure allows a more efficient allocation of the transmission power to data subcarriers when compared to conventional OFDM, and provides improved error performance. However, this subcarrier nulling procedure can be considered inefficient in terms of the spectral efficiency, particularly for higher order modulations. To solve this issue, as a novel technique, dual-mode OFDM with index modulation (DM-OFDM) has been recently proposed in [5] by filling the null subcarriers with an additional distinguishable symbol mapping procedure. This brings an improvement in terms of the throughput and increases the spectral efficiency. In the literature, OFDM-IM based studies include only computer simulation or theoretical analysis based performance results, and their real-time experimental performance is yet to be investigated. Specifically, their performance under CFO and real-time impairments cannot be properly stated. However, to assess the potential of IM-based waveforms for next-generation wireless networks, a real-time analysis becomes essential.

Our major contributions in this study are summarized as given below:

- OFDM-IM and DM-OFDM techniques are implemented in real-time and the performance of these techniques is evaluated in order to understand their behavior under hardware related impairments. By using software defined radio (SDR) technology, real-time implementations are performed. Two National Instruments (NI) USRP-2921 nodes are used as the transmitter and the receiver nodes. Moreover, NI PXI-6683H timing and synchronization module is used as a synchronization source for the transmitter node. GPSDO module is also used with the receiver node as a source of synchronization signal to this node. In order to provide the required clock signals and to create a more realistic synchronization between nodes, two separate synchronization sources are preferred. In this way, the performance of OFDM-IM and DM-OFDM is observed under real-time CFO and timing offset (TO) impairments.
- As a combined version of OFDM-IM and DM-OFDM, a hybrid OFDM-IM (H-OFDM-IM) scheme is proposed. H-OFDM-IM can be seen as a compression technique for OFDM-IM to manage the resources more effectively. H-OFDM-IM provides improvement in both spectral containment and error performance, as verified with both experiments and Monte Carlo simulation results. With its real-time friendly features, H-OFDM-IM appears as a good candidate for next-generation networks and provides an improved performance over both OFDM-IM and OFDM.

The rest of the paper is organized as follows. In Section II, the related studies in the literature are summarized and some important contributions are highlighted. In Section III, the system models of the implemented and the proposed techniques are explained. Then in Section IV, the technical details of the implemented testbeds are given. After presenting computer simulation and test results in Section V, the paper is concluded in Section VI. Main abbreviations that are used in this study are summarized in Table 1.

TABLE 1. List of frequently used abbreviations.

Additive white Gaussian noise	AWGN
Bit error rate	BER
Carrier frequency offset	CFO
Cyclic prefix	CP
Dual-mode OFDM with index modulation	DM-OFDM
Fast Fourier transform	FFT
Hybrid OFDM-IM	H-OFDM-IM
Index modulation	IM
Inter-carrier interference	ICI
Inverse fast Fourier transform	IFFT
Log-likelihood ratio	LLR
Maximum-likelihood	ML
Orthogonal frequency division multiplexing	OFDM
OFDM with index modulation	OFDM-IM
Peak-to-average power ratio	PAPR
Signal-to-noise ratio	SNR
Software defined radio	SDR
Timing offset	TO
Virtual instrument	VI

II. RELATED WORKS

In this section, we briefly cover the existing studies on OFDM-IM, which has attracted significant interest in the recent years. OFDM-IM is a promising form of IM, which is a novel digital modulation format that considers the transmit entities such as transmit antennas, subcarriers, radio frequency mirrors, relays and modulation types for the transmission of additional information bits [6], [7]. Due to its attractive advantages over classical OFDM, such as improved error performance, a more flexible structure, lower PAPR as well as higher robustness to inter-carrier interference (ICI), many researchers have explored the potential of OFDM-IM and its variants. In [8], OFDM with generalized index modulation (OFDM-GIM) scheme is proposed, where a flexible subcarrier activation procedure is applied in comparison to the fixed structure of OFDM-IM. With the proposed detector, this scheme provides an improved spectral efficiency by sacrificing the error performance, which is validated with computer simulations. Coordinate interleaving is introduced for active subcarriers of OFDM-IM in order

to improve the achievable diversity order in [9]. In [10], an improved maximum-likelihood (ML) detector is proposed for OFDM with the in-phase/quadrature index modulation (OFDM-I/Q-IM) scheme, and both asymptotic average bit error probability (ABEP) and exact coding gain expressions are provided. As shown by computer simulations, this scheme provides improved error performance and spectral efficiency over the OFDM-IM scheme. A linear constellation precoded OFDM-IM scheme is also introduced in [11] to harvest an additional diversity gain. DM-OFDM is proposed in [5] to improve the spectral efficiency and activate the nulled subcarriers of the OFDM-IM scheme. This procedure is applied by activating nulled subcarriers with an additional distinguishable signal mapping. According to computer simulations, a noticeable spectral efficiency improvement is obtained with a good level of error performance.

As a further improvement over DM-OFDM, generalized DM-OFDM (GDM-OFDM) is proposed in [12]. Accordingly, the number of active subcarriers belonging to corresponding signal constellation is not kept constant. Moreover, inverleaving is utilized to improve the error performance of this scheme at low signal-to-noise ratio (SNR). Such a procedure brings a spectral efficiency improvement by sacrificing the error performance, as validated through computer simulations. More recently, by using the full permutation of modes to convey a higher number of IM bits, the multiple-mode OFDM-IM scheme is proposed in [13]. In [14], IM is adopted to generalized frequency division multiplexing (GFDM) technique, which has subcarrier-wise filtering and non-orthogonal subcarrier localization, and GFDM-IM is proposed. Performance of this scheme is compared to that of GFDM and an improved error performance is obtained. Finally, a framework is proposed in [15] by integrating GFDM with space and frequency IM schemes to provide flexible waveforms for future wireless networks.

Besides single-input single-output systems, IM is also adopted to multiple-input multiple-output OFDM (MIMO-OFDM) systems and MIMO-OFDM-IM is proposed in [16]. It is shown via comprehensive computer simulations that MIMO-OFDM-IM performs better than MIMO-OFDM for several configurations. In [17], four different detectors are proposed for MIMO-OFDM-IM and their error performance comparisons with MIMO-OFDM are provided. As an important contribution, error performance of the MIMO-OFDM-IM scheme is evaluated in a realistic LTE channel by considering channel estimation errors and it is shown that this scheme can outperform MIMO-OFDM. A space-frequency coded IM scheme is also proposed to obtain a better performance than MIMO-OFDM-IM with transmit diversity [18]. More recently, sequential Monte Carlo theory based, low-complexity, and near optimal detection algorithms are proposed for MIMO-OFDM-IM [19].

In [20], the energy efficiency of OFDM-IM is investigated and an information-theoretical analysis is provided. A strategy that provides an improved energy efficiency is proposed for OFDM-IM, where the improvement is shown through computer simulations. In [21], subcarrier-level interleaving is adopted to the OFDM-IM scheme and OFDM with interleaved sucarrier-index modulation (OFDM-ISIM) is proposed. According to the provided analyses, this scheme provides a higher performance than OFDM-IM when lower order constellations are utilized. In order to improve the error performance of OFDM-IM, an equiprobable subcarrier activation method, which allows the activation of all subcarriers with almost equal probability, is proposed in [22]. An improved version of OFDM-IM is introduced in [23], where subblocks are created in an adaptive manner. In this scheme, different mappings and active subcarrier selection procedures can be implemented within each subblock. Transmission structure is given and according to the computer simulations, and an improved efficiency and error performance can be obtained. OFDM with type-2 generalized index modulation (OFDM-GIM2) scheme of [24], is targeted in [25] where IM is independently implemented to the in-phase and quadrature components of subcarriers. An improved version of OFDM-GIM2 is proposed by joint in-phase/quadrature IM and a higher spectral efficiency is obtained. A subcarrier allocation scheme is proposed for OFDM-IM in [26], where the average minimum Euclidean distance is maximized to improve the error performance. Moreover, a simple subcarrier allocation scheme is also proposed as a low-complexity algorithm. As shown with the provided results, significant performance improvements over OFDM-IM can be obtained. In [27], the performance of OFDM-IM is analyzed by considering metrics such as Euclidean distance and PAPR. Accordingly, an OFDM-IM scheme that provides a better error rate than OFDM at low throughput, is constructed. Moreover, as proven with extensive theoretical analysis and computer simulations, the PAPR performance of OFDM-IM is quite similar to that of OFDM's while considering Gaussian distributed input symbols.

SM-OFDM with subcarrier IM (ISM-OFDM), is proposed for vehicle-to-vehicle and vehicle-to-infrastructure (V2X) communications in [28]. In vehicular communications, in order to obtain an improved performance over OFDM-IM, quadrature index modulated OFDM is proposed in [29]. It is shown via computer simulation results that the proposed scheme outperforms OFDM-IM. In [30], ICI cancellation technique is adopted to the OFDM-IM with the aim of improving the ICI cancellation level in V2X channels. According to the computer simulation results, this scheme outperforms both OFDM and OFDM-IM. In [31], OFDM-IM with subcarrier-level interleaving is adopted to the vehicle-to-infrastructure (V2I) communications to provide performance improvement over OFDM and OFDM-IM schemes. It is validated through computer simulations that OFDM-IM provides improvement over classical OFDM for V2I communications.

In [32], vulnerability of underwater acoustic (UWA) communications systems to ICI is targeted and a procedure is proposed for OFDM-IM. It is shown through computer simulations that this scheme outperforms existing schemes. PAPR and ICI performance of OFDM-IM is also analyzed

in [33], where a better performance than OFDM is obtained. In [34], in order to improve OFDM-IM's vulnerability against ICI, new methods to cancel ICI are proposed for OFDM-IM. As a consequence, the spectral efficiency decreases, however, this scheme provides a better error performance than OFDM. Error probability analysis in the presence of CFO, is targeted for OFDM-IM in [35]. As validated with theoretical analysis and computer simulations, OFDM-IM provides a better performance than OFDM.

In summary, OFDM-IM and its variations have been studied from various perspectives in the past years. However, to the best of authors' knowledge, there is no study that targets real-time performance of OFDM-IM. As will be explained in the following sections, this study deals with this interesting issue, which has a paramount importance to assess the potential of IM-based waveforms for next-generation networks.

III. SYSTEM MODEL

In this section, the system models of the implemented OFDM-IM and DM-OFDM schemes are given. The proposed H-OFDM-IM scheme is also explained.

A. SYSTEM MODELS FOR OFDM-IM AND DM-OFDM

In this subsection, we introduce the system models of OFDM-IM and DM-OFDM schemes that are used in the practical implementation. It should be noted that the DM-OFDM system model, which is given in detail below, is also valid for OFDM-IM when the second DM-OFDM signal constellation contains a single element that is zero. According to the DM-OFDM's transmitter model proposed in [5], p groups are created by splitting a total of m information bits into portions of g bits, i.e., $p = m/g$. In classical OFDM-IM scheme, in each group, the first g_1 bits of g bits select the index set of the active subcarriers and, the following g_2 bits are modulated with the corresponding modulation and form the active subcarriers. However, in DM-OFDM, additional information bits can also be transmitted and the data rate can be improved. Accordingly, inactive subcarriers are activated by modulating them with a different constellation. Thus, there are two index subsets for each constellation, which are orthogonal to each other and activate all available subcarriers in the corresponding group. In other words, the determination of the first index set is sufficient to decide on the indices of the second constellation.

With index selection and activation of subcarriers, an OFDM subblock of length $l = N/p$ is created, where N represents the size of the inverse fast Fourier transform (IFFT). Corresponding index sets for the first and the second constellations are denoted by $\mathcal{I}_A$ and $\mathcal{I}_B$, respectively. Similar to the sets given in [5], constellations that are used in this study, are determined as $\mathcal{M}_A = \{-1-j, 1-j, 1+j, -1+j\}$ and $\mathcal{M}_B = \{1+\sqrt{3}, (1+\sqrt{3})j, -1-\sqrt{3}, -(1+\sqrt{3})j\}$, respectively. If the number of subcarriers that contain symbols from $\mathcal{M}_A$ constellation set is equal to k and the number of remaining subcarriers is equal to $l-k$, the corresponding numbers of IM and ordinary modulation bits can be calculated as

$$g_1 = \left\lfloor \log_2\left(\frac{l!}{(l-k)!k!}\right) \right\rfloor, \tag{1}$$

$$g_2 = k\log_2(M_A) + (l-k)\log_2(M_B), \tag{2}$$

where $\lfloor\cdot\rfloor$ represents the floor operator, and M_A and M_B represent the sizes of the corresponding constellations. In this implementation study, these parameters are selected as $g_1 = 2$, $l = 4$ and $k = 2$ and for these parameters, index patterns are determined as shown in Table 2. In the table, $S_A^{(i)}$ and $S_B^{(i)}$ represent the two symbols ($i = 1, 2$) selected from the corresponding constellations, $\mathcal{M}_A$ and $\mathcal{M}_B$. Then, the created subblocks are concatenated as

$$X_d\big[(\beta-1)l+\alpha\big] = X^{\beta}[\alpha], \tag{3}$$

for $\alpha = 1, 2, \ldots l$, $\beta = 1, 2, \ldots p$, where $X^{\beta}[\alpha]$ represents the α^{th} subcarrier of the β^{th} subblock. Before the IFFT operation, reference subcarriers are inserted into subblocks in accordance with a comb-type pilot allocation. As shown in [36], comb-type pilot allocation can be done by inserting $\mathbb{K}_p$ pilot subcarriers into $\mathbb{K}_d$ data subcarriers for channel estimation such that

$$X\big[\mathbb{k}\big] = X\big[(a-1)V+v\big] = \begin{cases} X_p\big[a\big], & v = 1 \\ X_d\big[(a-1)(V-1)+v-1\big], & v = 2, 3, \ldots, V, \end{cases} \tag{4}$$

where $X[\mathbb{k}]$ stand for the frequency-domain OFDM samples with the subcarrier indices of $\mathbb{k} = 1, 2, \ldots, \mathbb{K}_p + \mathbb{K}_d$, $X_p\big[a\big]$ represents the a^{th} pilot subcarrier with $a = 1, 2, \ldots, \mathbb{K}_p$ and, V denotes the ratio of total number of subcarriers to the pilot subcarriers such that $V = \frac{\mathbb{K}_d+\mathbb{K}_p}{\mathbb{K}_p}$. Then, these frequency domain symbols can be transformed into time domain as

$$x[n] = \frac{1}{\sqrt{\mathbb{K}}} \sum_{\mathbb{k}=1}^{\mathbb{K}} X\,[\mathbb{K}]\, e^{j2\pi(\mathbb{k}-1)n/\mathbb{K}}, \quad n = 1, 2, \ldots, N, \tag{5}$$

where $\mathbb{K}$ is the total number of subcarriers, i.e., $\mathbb{K} = \mathbb{K}_d + \mathbb{K}_p$. In order to estimate as well as compensate CFO and TO, an algorithm should be utilized in real-time. Van de Beek algorithm in [37] makes use of correlation with CP to obtain symbol timing and maximum likelihood

TABLE 2. Look-up table for index selection with parameters of $g_1 = 2$, $l = 4$ and $k = 2$.

Index Bits	Indices	Subblocks
[0, 0]	[1, 2]	$[S_A{}^{(1)}, S_A{}^{(2)}, S_B{}^{(1)}, S_B{}^{(2)}]$
[0, 1]	[1, 3]	$[S_A{}^{(1)}, S_B{}^{(1)}, S_A{}^{(2)}, S_B{}^{(2)}]$
[1, 0]	[1, 4]	$[S_A{}^{(1)}, S_B{}^{(1)}, S_B{}^{(2)}, S_A{}^{(2)}]$
[1, 1]	[2, 4]	$[S_B{}^{(1)}, S_A{}^{(1)}, S_B{}^{(2)}, S_A{}^{(2)}]$

CFO estimates. Received signal with CFO and TO can be represented as

$$y[n] = e^{j2\pi n\varepsilon} h[n] * x[n-\theta] + w[n], \tag{6}$$

where $n = 1, 2, \ldots, N + N_{CP}$, $*$ is the linear convolution operator, N_{CP} is the length of CP samples, $h[n]$ represents the channel impulse response and $w[n]$ represents the additive white Gaussian noise (AWGN) samples. Furthermore, ε and θ represent CFO and TO, respectively. According to [37], a log-likelihood function is maximized in order to obtain CFO and TO, which can be shown as [37]

$$\Lambda(\theta, \epsilon) = |\gamma(\theta)| cos(2\pi\epsilon + \angle\gamma(\theta)) - \rho\Phi(\theta), \tag{7}$$

where γ is the consecutive correlation between samples, Φ is an energy term and ρ is the coefficient of correlation between N spaced samples. After the maximization, the estimates of ε and θ can be obtained as

$$\hat{\varepsilon}_{ML}(\theta) = -\frac{1}{2\pi}\angle\gamma(\theta), \tag{8}$$

$$\hat{\theta}_{ML} = \arg\max_{\theta}\{|\gamma(\theta)| - \rho\Phi(\theta)\}. \tag{9}$$

With these estimates, CFO and TO are compensated and CP is removed. After the CP removal, frequency domain representation of the received signal can be obtained with N-point FFT such as

$$Y[\mathbb{k}] = \frac{1}{\sqrt{N}} \sum_{n=1}^{N} y[n] e^{-j2\pi\mathbb{k}(n-1)/N}. \tag{10}$$

$Y[\mathbb{k}]$ can also be represented as

$$Y[\mathbb{k}] = H[\mathbb{k}]X[\mathbb{k}] + W[\mathbb{k}], \tag{11}$$

where $H[\mathbb{k}]$ and $W[\mathbb{k}]$ are frequency domain representations of $h[n]$ and $w[n]$, respectively. After the separation of data and pilot subcarriers, channel estimation is implemented. Channel coefficients observed on the received pilot subcarriers $Y_p[a]$, that are separated from (11), can be estimated with zero-forcing method such that

$$H_p[a] = \frac{Y_p[a]}{X_p[a]}, \quad a = 1, 2, \ldots \mathbb{K}_p. \tag{12}$$

Then, the channel coefficient on $\mathbb{k}^{\text{th}}$ data subcarrier can be estimated by implementing one-dimensional interpolation [38] with $H_p[a]$ such that

$$H_d[\mathbb{k}] = (H_p[a+1] - H_p[a])\frac{v}{V} + H_p[a]. \tag{13}$$

Then, the separated data components from (11), can be written as

$$Y_d[\mathbb{k}] = H_d[\mathbb{k}]X_d[\mathbb{k}] + W[\mathbb{k}]. \tag{14}$$

1) REDUCED-COMPLEXITY ML DETECTOR

In order to obtain a high detection performance, a reduced-complexity ML detector is proposed for the DM-OFDM scheme. Accordingly, as the first step, transmitted symbols at index sets of the first and second constellations are estimated as

$$\hat{X}_{d,A}[\mathbb{k}] = \arg\min_{S_A(m)\in\mathcal{M}_A} \left|Y_d[\mathbb{k}] - H_d[\mathbb{k}]S_A(m)\right|^2, \tag{15}$$

$$\hat{X}_{d,B}[\mathbb{k}] = \arg\min_{S_B(q)\in\mathcal{M}_B} \left|Y_d[\mathbb{k}] - H_d[\mathbb{k}]S_B(q)\right|^2, \tag{16}$$

where $S_A(m)$ and $S_B(q)$ are the m^{th} and q^{th} elements of the constellations $\mathcal{M}_A$ and $\mathcal{M}_B$, respectively. Then, the following metric is calculated for all subcarriers of the corresponding subblock as

$$ML[\mathbb{k}] = \left|Y_d[\mathbb{k}] - H_d[\mathbb{k}]\hat{X}_{d,A}[\mathbb{k}]\right|^2 - \left|Y_d[\mathbb{k}] - H_d[\mathbb{k}]\hat{X}_{d,B}[\mathbb{k}]\right|^2. \tag{17}$$

Afterwards, in the corresponding subblock, all $ML[\mathbb{k}]$ values are sorted in an ascending order and, in accordance with the look-up table, indices of the first constellation are determined by evaluating the first values. Remaining indices in subblock are determined from the second constellation and transmitted symbols are estimated for each constellation from (15) or (16).

2) LLR DETECTOR

Alternatively, the reduced-complexity log-likelihood ratio (LLR) detector, which is modeled in [5], is considered. Accordingly, the logarithm of the ratio of posteriori probabilities is calculated in order to separate the subcarriers from two different constellations. This is realized as

$$\gamma_{\mathbb{k}} = \ln\left(\frac{\sum_{m=1}^{M_A} \Pr\left(X_d[\mathbb{k}] = S_A(m)|Y_d[\mathbb{k}]\right)}{\sum_{q=1}^{M_B} \Pr\left(X_d[\mathbb{k}] = S_B(q)|Y_d[\mathbb{k}]\right)}\right). \tag{18}$$

It is clear that at high SNR, $\gamma_{\mathbb{k}}$ is positive if the subcarrier at corresponding index is modulated with the first constellation, and it is negative if the subcarriers are modulated with the other constellation. The LLR value of $\gamma_{\mathbb{k}}$ is calculated with this algorithm and then, transmitted symbols can be estimated as

$$\hat{X}_d[\mathbb{k}] = \begin{cases} \arg\min_{S_A(m)\in\mathcal{M}_A} \left|Y_d[\mathbb{k}] - H_d[\mathbb{k}]S_A(m)\right|^2, & \tilde{\gamma}_{\mathbb{k}} = +1, \\ \arg\min_{S_B(q)\in\mathcal{M}_B} \left|Y_d[\mathbb{k}] - H_d[\mathbb{k}]S_B(q)\right|^2, & \tilde{\gamma}_{\mathbb{k}} = -1, \end{cases} \tag{19}$$

where $\tilde{\gamma}_{\mathbb{k}}$ represents the signs of $\gamma_{\mathbb{k}}$, i.e., $\tilde{\gamma}_{\mathbb{k}} = \text{sgn}(\gamma_{\mathbb{k}})$. For each subblock, by following the patterns in the look-up table, IM bits can be determined by using the obtained values of $\tilde{\gamma}_{\mathbb{k}}$.

B. H-OFDM-IM SYSTEM MODEL

As a hybrid version of OFDM-IM and DM-OFDM, a new waveform, which is named as H-OFDM-IM, is proposed

in this study. Accordingly, the OFDM scheme in which all subcarriers are active, is considered. Improvements in both spectral containment and error performance are targeted. Since inactive subcarriers in OFDM-IM provides additional transmit power for the active ones, a higher number of inactive subcarriers is desired in order to improve the error performance at the cost of a reduced data rate. Moreover, as a unique approach, the positions of these inactive subcarriers can be selected in a way that sidelobe attenuation levels are decreased.

Combination of these two design issues would bring improved sidelobe attenuation and error performance. In H-OFDM-IM, some subblocks at the beginning and at the end of the OFDM symbol are inactivated and are constructed of only nulled subcarriers. A number of subblocks are created as OFDM-IM subblocks, while the remaining subblocks are created as DM-OFDM subblocks in order to provide an equal data rate with that of classical OFDM. The number of these subblocks are determined in accordance with the targeted sidelobe attenuation performance and to keep the same data rate. These different subblocks can be concatenated as

$$X_d\big[(\beta-1)l+\alpha\big]=\begin{cases}0, & \alpha\in B_z,\\ X^{\beta}[\alpha], & \alpha\in B_{im}\cup B_{dm},\end{cases} \tag{20}$$

where B_z, B_{im} and B_{dm} represent the subblocks belonging to nulled subblocks, OFDM-IM subblocks and DM-OFDM subblocks, respectively. Moreover B_z, B_{im} and B_{dm} represent the numbers of these subblocks, respectively. For OFDM-IM subblocks, the look-up table in Table 3 is utilized and the procedure in [2] is implemented.

TABLE 3. Look-up table for index selection in OFDM-IM, with parameters of $g_1 = 2$, $l = 4$ and $k = 3$.

Index Bits	Indices	Subblocks
[0, 0]	[1, 2, 3]	$[S_A{}^{(1)}, S_A{}^{(2)}, S_A{}^{(3)}, 0]$
[0, 1]	[1, 2, 4]	$[S_A{}^{(1)}, S_A{}^{(2)}, 0, S_A{}^{(3)}]$
[1, 0]	[1, 3, 4]	$[S_A{}^{(1)}, 0, S_A{}^{(2)}, S_A{}^{(3)}]$
[1, 1]	[2, 3, 4]	$[0, S_A{}^{(1)}, S_A{}^{(2)}, S_A{}^{(3)}]$

At the receiver side, the following LLR expression is calculated for a given OFDM-IM subblock

$$\gamma_{\mathbb{k}}=\ln\left(\frac{\sum_{m=1}^{M_A}\Pr\big(X_d[\mathbb{k}]=S_A(m)|Y_d[\mathbb{k}]\big)}{\Pr\big(X_d[\mathbb{k}]=0|Y_d[\mathbb{k}]\big)}\right). \tag{21}$$

Afterwards, positive $\gamma_{\mathbb{k}}$ determines the active subcarrier and the corresponding bits that are used in index selection are estimated in accordance with the look-up table. Then, the transmitted symbols at active indexes are estimated as

$$\hat{X}_d[\mathbb{k}]=\begin{cases}\arg\min\limits_{S_A(m)\in\mathcal{M}_A}\big|Y_d[\mathbb{k}]-H_d[\mathbb{k}]S_A(m)\big|^2, & \tilde{\gamma}_{\mathbb{k}}=+1,\\ 0, & \tilde{\gamma}_{\mathbb{k}}=-1.\end{cases} \tag{22}$$

For DM-OFDM subblocks, the procedure in the previous subsection is applied and the patterns in the look-up table are tracked. Then, data bits are estimated.

IV. TESTBED DETAILS

In this section, we provide the technical details of the transmitter and receiver testbeds. In Fig. 1, the realized experimental setup is shown.

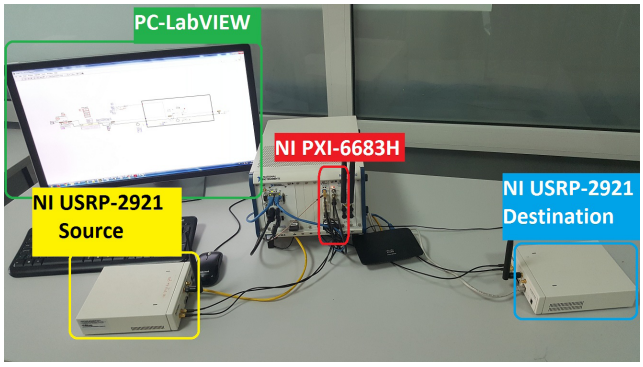

FIGURE 1. Experimental setup used in real-time implementation.

A. TRANSMITTER DETAILS

1) PILOT TONES FOR CHANNEL ESTIMATION

In order to estimate and track the channel, comb-type channel estimation method with one dimensional linear interpolation is used. Accordingly, a group of subcarriers are used as the pilot tones in accordance with the considered ratio of number of data subcarriers and pilot subcarriers. In this implementation, this ratio is considered to be 8, i.e, one pilot tone is used for 8 data subcarriers.

2) SYMBOL STRUCTURE

The structure of the considered OFDM symbol is shown in Table 4 with the corresponding system parameters. Accordingly, data subcarriers, pilot subcarriers and nulled subcarriers are inserted, where we have 112 nulled subcarriers at the beginning, one nulled subcarrier at the center and 111 nulled subcarriers at the end of the symbol. The symbol is created and IFFT operation with a length of 512 is realized. After the IFFT operation, the CP portion is added. The length of CP portion is 88 samples, therefore, CP overhead in time domain signal is approximately 17%. With the CP addition, time domain signal is created.

3) SOFTWARE AND HARDWARE CONFIGURATION

In order to transmit the generated symbols with the USRP node, related configurations are constructed. Programming is achieved by using LabVIEW's virtual instrument (VI) components. To start and manage the transmission session with USRP, 'Open Tx Session VI', 'Configure Signal VI', 'Set Time VI', 'Write Tx Data VI' and 'Close Session VI' from the USRP library in LabVIEW are used [39]. Configurations of the transmission parameters such as gain and

TABLE 4. Measurement setup parameters.

Carrier frequency	2.45 GHz
I/Q data rate	10^6 samples/sec
Sampling rate (f_s)	1.25×10^6 samples/sec
Utilized modulation / DM-OFDM	4-QAM
Utilized modulation / OFDM-IM	16-QAM
Number of data subcarriers ($\mathbb{K}_d$)	256
Number of reference subcarriers ($\mathbb{K}_p$)	32
Number of source / destination node	1 / 1
Zero padding / FFT length (N)	224 / 512
CP length (N_{CP})	88
Simulation Channel	4-tap Rician, uniform power delay profile, $K = 5$
Simulated H-OFDM-IM schemes	$B_z = 4$ / $B_z = 8$ / $B_z = 12$
Distance between Tx and Rx nodes	150 cm

carrier frequency, are set with 'Configure Signal VI'. The configured parameters are shown in Table 4. Additionally, synchronization configuration is performed by using related VI component. Here, the reference frequency source and clock source of USRP are configured and NI PXI-6683H module is used as a reference. Since NI PXI-6683H module is a separate one that is integrated to NI PXIe-1082 chassis, the module and USRP node are connected with RF cables. A 10 MHz clock signal and related time signal are transmitted via these RF cables. With these steps, the transmitter is configured and used in experiments to implement data transmission.

B. RECEIVER DETAILS

1) CFO AND TO ESTIMATION

After reception of data from the channel, first, CFO and TO are estimated. Van de Beek algorithm [37] is used for this purpose. This algorithm exploits the correlation arising from the CP portion and obtains symbol timing and maximum likelihood CFO estimates. Since the received signal contains repetitive parts, which are CP portion and the portion at the end of the symbol, autocorrelation can be utilized to obtain offset estimates. By this repetition, both the start of the symbol and CFO can be estimated. By the estimation of TO, the CP portion is removed and the estimated CFO is fixed.

2) CHANNEL ESTIMATION

After the FFT operation, data and pilot subcarriers are extracted. By following the pilot insertion procedure in the transmitter side, data and pilot subcarriers are separated. With one-dimensional linear interpolation, channel coefficients are estimated. Then, the estimated channel coefficients are given as input to OFDM-IM and DM-OFDM demodulation algorithms.

3) SNR ESTIMATION

For SNR estimation, which is crucial for the comparison of experiment results with the results obtained by computer simulations, the method proposed in [40] is considered. Accordingly, instantaneous signal power can be estimated by the evaluation of the best hypotheses of the received noisy and noise-free signals. Detection procedure of OFDM-IM scheme can be considered as an example. Accordingly, the instantaneous noise power can be computed as

$$Z_d[\mathbb{k}] = |Y_d[\mathbb{k}] - \hat{X}_d[\mathbb{k}]H_d[\mathbb{k}]|^2. \tag{23}$$

Since this expression is computed on a subcarrier-basis, to obtain the average noise power, results of each subcarrier are averaged as

$$\tilde{Z}_d = \frac{1}{\mathbb{K}} \sum_{l=1}^{\mathbb{K}} Z_d[\mathbb{k}]. \tag{24}$$

After computation of the noise power, average signal power can be computed according to

$$\tilde{P}_d = \frac{1}{\mathbb{K}} \sum_{l=1}^{\mathbb{K}} Y_d[\mathbb{k}]. \tag{25}$$

Finally, SNR can be estimated as

$$\tilde{SNR}_d = \frac{\tilde{P}_d}{\tilde{Z}_d}. \tag{26}$$

4) SOFTWARE AND HARDWARE CONFIGURATION

To implement the reception process on the USRP device, VIs from USRP VI library, which are 'Open Rx Session VI', 'Configure Signal VI', 'Set Time VI', 'Initiate VI', 'Fetch Rx Data VI', 'Abort VI', 'Close Session VI', are utilized [39]. Just as in the transmitter side, transmission parameters are allocated by using 'Configure Signal VI'. In order to synchronize the receiver node with the transmitter node, synchronization configuration is performed by using the same VI. Then, the data received by USRP is transferred to the host computer by using the 'Fetch Rx Data VI' and the data is processed at OFDM-IM and DM-OFDM demodulation VIs.

V. SIMULATION AND TEST RESULTS

In this section, the results of conducted computer simulations and real-time experiments are presented and some important points are highlighted. Performances of different systems are measured in terms of bit error rate (BER) and spectral containment. In order to observe the differences in performances, real-time experiments are conducted for OFDM-IM and DM-OFDM schemes by also experimenting two different k parameters. Moreover, the same schemes are also evaluated with computer simulations and these results are jointly presented to observe the differences between the ideal and real-time environments. Performances of OFDM, OFDM-IM and H-OFDM-IM schemes are compared with real-time experiments and computer simulations by experimenting two different k parameters and three different nulled subblock setups. Lastly, spectral containments of OFDM, OFDM-IM and H-OFDM-IM are demonstrated to highlight the benefits of the H-OFDM-IM scheme, by also evaluating different parameters.

The considered symbol structure and the determined parameters are shown in Table 4. In the results, the spectral

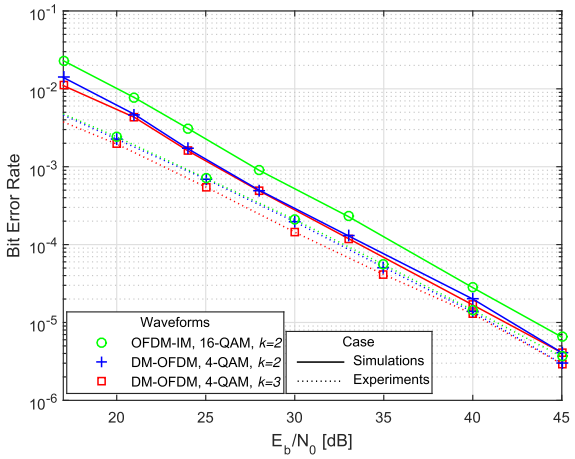

FIGURE 2. Performance results for OFDM-IM and DM-OFDM schemes, for $k = 2$ and $k = 3$, and a spectral efficiency of 0.225 bits/s/Hz.

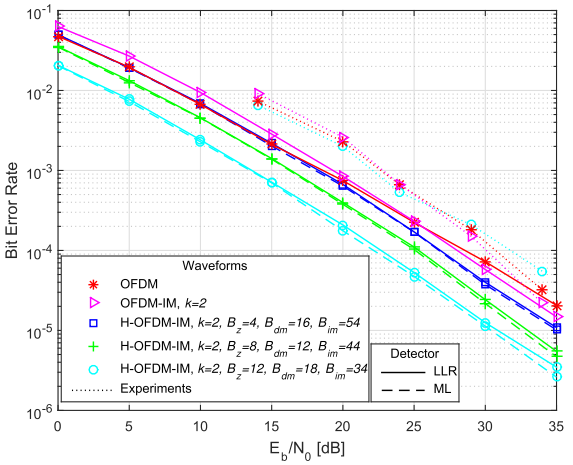

FIGURE 3. Performance results for OFDM, OFDM-IM and H-OFDM-IM schemes, for $k = 2$, and the spectral efficiency is equal to 0.64 bits/s/Hz.

efficiency of the corresponding system is also computed as the division of data rate to transmission bandwidth, where data rate R is equal to $\frac{p(g_1+g_2)}{T_s}$ bits/sec, considering a symbol duration of T_s seconds. In order to make a fair comparison, channel characteristics of the testbed are measured, and the channel in the computer simulations is determined in accordance with these measurement results. Accordingly, a four-tap Rician channel with uniform power delay profile and K-factor of 5 is determined.

A. RESULTS FOR OFDM-IM VS DM-OFDM

OFDM-IM and DM-OFDM schemes are evaluated with computer simulations and real-time experiments. Error performance results of these schemes are demonstrated in Fig. 2. Due to the difficulty of accurate allocation of the desired transmission power, experimented E_b/N_0 interval is obtained as 17 to 45 dB, where E_b is the average transmitted energy per bit and N_0 is the noise power spectral density. As the second difficulty, due to limited node distance that stems from the lengths of RF cables used in the synchronization solution, lower E_b/N_0 values cannot be experimented. DM-OFDM schemes are implemented with 4-QAM, and for a fair comparison, OFDM-IM scheme is implemented with 16-QAM and $k = 2$ to keep the same data rate. Here, the bandwidth of transmission is equal to 1 MHz, subcarrier spacing is approximately 3.5 kHz, and symbol duration is equal to 2.85 ms. Therefore, the system data rate becomes 225 kbit/s and the spectral efficiency is 0.225 bits/s/Hz. Different k parameters are also utilized for the DM-OFDM scheme.

As observed with real-time test results, the DM-OFDM scheme provides a better error performance than the OFDM-IM scheme. Moreover, as expected, a higher value of k improves the performance. Since k parameter represents the number of subcarriers that belong to the first constellation that contains subcarriers with lower power (compared to the second constellation), at the same power consumption, a higher value of k allocates more power to all data

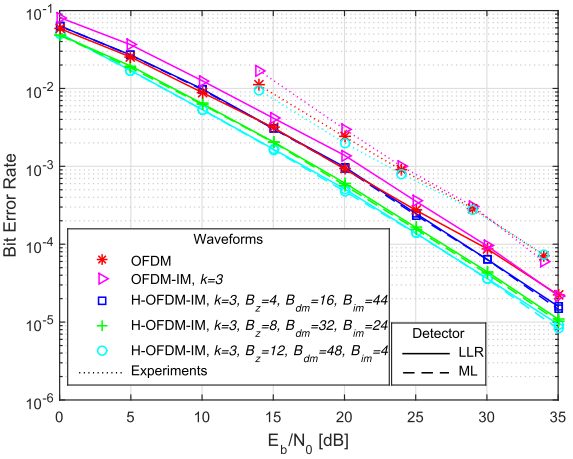

FIGURE 4. Performance results for OFDM, OFDM-IM and H-OFDM-IM schemes, for $k = 3$, and the spectral efficiency is equal to 0.85 bits/s/Hz.

subcarriers. These schemes are also compared with computer simulations. The same observations are also valid for these results, where the difference between two different DM-OFDM schemes decreases at higher E_b/N_0 values. Compared to computer simulation results, real-time results are inferior at lower E_b/N_0 values, and after E_b/N_0 value of 30 dB, results start to converge. It is clear that at higher E_b/N_0 values, real-time impairments cause fewer bit errors. It is also clear that DM-OFDM scheme provides an improved BER performance also in real-time and is not significantly affected from real-time impairments at high E_b/N_0 values.

B. RESULTS FOR OFDM, OFDM-IM AND H-OFDM-IM

BER performances of OFDM, OFDM-IM and the proposed H-OFDM-IM schemes are evaluated with real-time experiments and compared with computer simulation results as demonstrated in Figs. 3 and 4, for $k = 2$ and $k = 3$, respectively. As explained earlier, the motivation behind the H-OFDM-IM scheme is to allocate the total power more effectively to obtain a better error performance and spectral

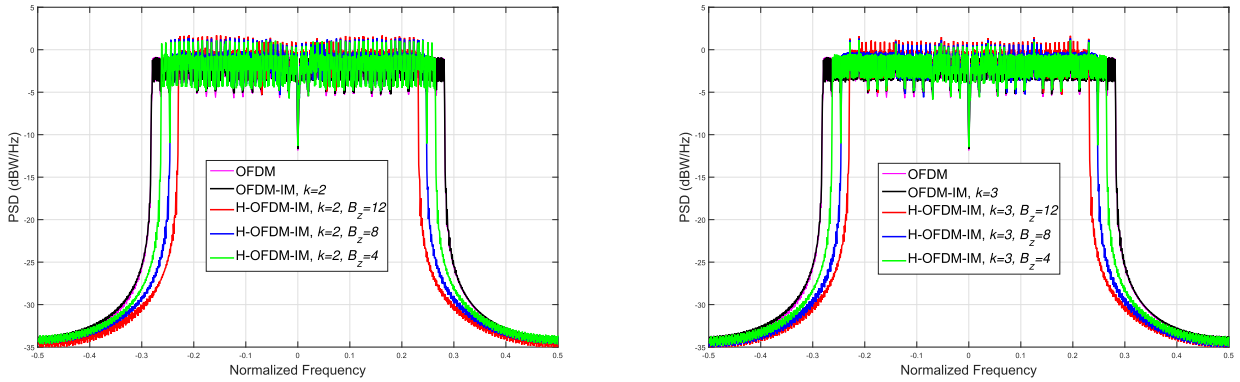

FIGURE 5. Spectral containment results of OFDM, OFDM-IM and H-OFDM-IM schemes, (a) for $k = 2$, (b) for $k = 3$, where the spectral efficiency is equal to 0.64 bits/s/Hz for (a), and 0.85 bits/s/Hz for (b), respectively.

containment. In order to validate this, three different B_z parameters are evaluated and the BER performance of H-OFDM-IM is compared with that of OFDM and OFDM-IM schemes. For H-OFDM-IM schemes, beside B_z values, corresponding B_{im} and B_{dm} values are also shown in the figures, but only B_z values will be mentioned for brevity. In all schemes, 4-QAM modulation is utilized in the OFDM symbol structure. First, as shown through computer simulations in Fig. 3, higher number of nulled subblocks, i.e., higher values of B_z, result in clear performance improvements over OFDM and OFDM-IM schemes. Especially when $B_z = 12$, BER performance advantages over the other schemes become more significant. Compared to OFDM-IM, OFDM performs better for lower E_b/N_0 values, but OFDM-IM outperforms OFDM after the E_b/N_0 value of 25 dB. Moreover, OFDM can only reach the performance of H-OFDM-IM scheme with $B_z = 4$, and this is only valid at lower E_b/N_0 values. After the E_b/N_0 value of 15 dB, OFDM scheme provides a worse BER performance. However, as shown with real-time experiment results, advantages of H-OFDM-IM scheme start to disappear in real-time, especially at E_b/N_0 values higher than 24 dB. In experiments, the H-OFDM-IM scheme with $B_z = 12$ is experimented. Performance loss of this scheme is resulted from the I/Q impairments stem from hardware issues and two different constellations cannot be effectively distinguished from each other. Moreover, OFDM-IM scheme provides the best performance at higher E_b/N_0 values. Compared to the simulation results, IM-based schemes show degraded performances and the use of OFDM is more favorable at low E_b/N_0 values. Again, I/Q impairments and channel estimation errors render index pattern detection procedure challenging and consequently, resulting performance degradation. However, techniques like interleaving, are not adopted to the IM-based schemes, and such tools could provide significant improvements, as shown in [2].

Second, as shown in Fig. 4, the same observations are also valid for the case of $k = 3$. When k is lower, more power is allocated to the active data subcarriers and an improved error performance obtained. Therefore, increasing k from 2 to 3 results in a degraded error performance, however, this increment provides an increased data rate. Moreover, advantages of higher values of B_z start to disappear. Since the data rate increases with $k = 3$ compared to the case of $k = 2$, increased number of DM-OFDM subblocks, i.e., B_{dm}, are created to keep the same data rate, and bit errors increase. In other words, a higher number of B_{im} is more desirable than that of B_{dm}. In computer simulation results, when compared to OFDM-IM, OFDM performs better, however, it cannot outperform H-OFDM-IM schemes. As observed in the previous results demonstrated in Fig. 3, real-time performance of H-OFDM-IM is again degraded and the schemes provide similar performances at higher E_b/N_0 values. In conclusion, H-OFDM-IM provides configuration flexibility and the desired error performance can be obtained with the corresponding parameter configuration.

C. SPECTRAL CONTAINMENT SIMULATION RESULTS FOR OFDM, OFDM-IM AND H-OFDM-IM

In order to assess the spectral containment benefits of the H-OFDM-IM scheme, spectral containment results of OFDM, OFDM-IM and H-OFDM-IM schemes are demonstrated in Fig. 5. These results are obtained by computer simulations with 1000 iterations for each scheme. In Fig. 5, averaged results of these iterations are shown. There are two groups of results, which are obtained for $k = 2$ and $k = 3$, respectively. First, for $k = 2$, when OFDM and OFDM-IM schemes are considered, their spectral containment results overlap and are almost identical. H-OFDM-IM scheme is again considered with three different configurations that are utilized in the computer simulations provided in previous subsection. With higher values of B_z, a more compact spectral containment is obtained and the frequency spectrum is used more efficiently. This is also valid for results that are obtained in the case of $k = 3$, and the results are almost the same except more confined amplitude variations at data subcarriers. The spectral containment benefit comes with a cost, where power levels of the subcarriers in DM-OFDM groups

are higher and distortions could arise due to these amplitude variations in some specific circumstances. However, obtained spectral containment benefit is quite significant and desirable. Especially for short-packet transmission applications, such as compressed spectrum, may bring important advantages into the system. As a noticeable property, this procedure can also bring an error performance improvement, which increases its applicability in next-generation technologies.

D. COMPLEXITY ANALYSIS

As explained in [2], OFDM-IM has a complexity on the order of $\mathcal{O}(lM)$ per subblock, where M is the size of the constellation. OFDM waveform has also the same implementation complexity. Moreover, LLR based detector, which is proposed for DM-OFDM, has a complexity on the order of $\mathcal{O}(l(M_A + M_B))$ per subblock in terms of metric calculations [5]. Comparing the implementation complexity of H-OFDM-IM with other waveforms on subblock basis would not be fair due to the presence of nulled subblocks. However, this can be realized on a symbol basis.

In the implementation procedure of H-OFDM-IM, DM-OFDM subblocks carry more bits than those of OFDM-IM subblocks, therefore these subblocks are not equal in terms of complexity. If both of them carry the same amount of bits, DM-OFDM subblocks bring an implementation advantage as explained. Thus, complexity of H-OFDM-IM waveform is higher than OFDM and OFDM-IM on a symbol basis. Implementation complexity of H-OFDM-IM is on the order of $\mathcal{O}(B_{im}lM_A + B_{dm}l(M_A + M_B))$ per H-OFDM-IM symbol. Symbol basis complexity levels of other waveforms can be easily calculated by utilizing the number of subblocks. With a numerical example, complexity difference can be understood more clearly. If we consider the case whose results are shown in Fig. 4, the LLR detection of OFDM and OFDM-IM requires 1024 metric calculations per OFDM symbol. For the case of H-OFDM-IM, 1216 metric calculations are required for LLR detection. Higher number B_{dm} values increase the complexity, however, the implementation complexity of H-OFDM-IM is not significantly higher, and improved spectral containment can be obtained.

VI. CONCLUSIONS

In this study, for the first time in the literature, OFDM-IM and DM-OFDM techniques have been implemented in real-time by using SDR nodes, in order to assess their suitability to real-time applications. Accordingly, implementation details have been provided and test results have been presented. Moreover, to provide a robust waveform for real-time use, H-OFDM-IM has been proposed and its comprehensive performance comparisons with OFDM and OFDM-IM have been presented. Accordingly, noticeable performance improvements over these techniques can be obtained with H-OFDM-IM. Feasible implementation details and performance results have been proposed for real-time applications. Furthermore, with the proposed effective technique, a beneficial perspective for real-time waveform design has been presented. As the future work, performance improvement of the H-OFDM-IM scheme and its enhanced versions in real-time will be targeted specifically focusing on real-time impairment effects.

REFERENCES

[1] Z. Ankarali, B. Peköz, and H. Arslan, "Flexible radio access beyond 5G: A future projection on waveform, numerology, and frame design principles," *IEEE Access*, vol. 5, pp. 18295–18309, 2017.
[2] E. Başar, Ü. Aygölü, E. Panayırcı, and H. V. Poor, "Orthogonal frequency division multiplexing with index modulation," *IEEE Trans. Signal Process.*, vol. 61, no. 22, pp. 5536–5549, Nov. 2013.
[3] R. Y. Mesleh, H. Haas, S. Sinanovic, C. W. Ahn, and S. Yun, "Spatial modulation," *IEEE Trans. Veh. Technol.*, vol. 57, no. 4, pp. 2228–2241, Jul. 2008.
[4] N. Serafimovski *et al.*, "Practical implementation of spatial modulation," *IEEE Trans. Veh. Technol.*, vol. 62, no. 9, pp. 4511–4523, Nov. 2013.
[5] T. Mao, Z. Wang, Q. Wang, S. Chen, and L. Hanzo, "Dual-mode index modulation aided OFDM," *IEEE Access*, vol. 5, pp. 50–60, 2017.
[6] E. Basar, "Index modulation techniques for 5G wireless networks," *IEEE Commun. Mag.*, vol. 54, no. 7, pp. 168–175, Jul. 2016.
[7] E. Basar, M. Wen, R. Mesleh, M. Di Renzo, Y. Xiao, and H. Haas, "Index modulation techniques for next-generation wireless networks," *IEEE Access*, vol. 5, pp. 16693–16746, 2017.
[8] R. Fan, Y. J. Yu, and Y. L. Guan, "Orthogonal frequency division multiplexing with generalized index modulation," in *Proc. IEEE Global Commun. Conf.*, Austin, TX, USA, Dec. 2014, pp. 3880–3885.
[9] E. Başar, "OFDM with index modulation using coordinate interleaving," *IEEE Wireless Commun. Lett.*, vol. 4, no. 4, pp. 381–384, Aug. 2015.
[10] B. Zheng, F. Chen, M. Wen, F. Ji, H. Yu, and Y. Liu, "Low-complexity ML detector and performance analysis for OFDM with in-phase/quadrature index modulation," *IEEE Commun. Lett.*, vol. 19, no. 11, pp. 1893–1896, Nov. 2015.
[11] M. Wen, B. Ye, E. Başar, Q. Li, and F. Ji, "Enhanced orthogonal frequency division multiplexing with index modulation," *IEEE Trans. Wireless Commun.*, vol. 16, no. 7, pp. 4786–4801, Jul. 2017.
[12] T. Mao, Q. Wang, and Z. Wang, "Generalized dual-mode index modulation aided OFDM," *IEEE Commun. Lett.*, vol. 21, no. 4, pp. 761–764, Apr. 2017.
[13] M. Wen, E. Başar, Q. Li, B. Zheng, and M. Zhang, "Multiple-mode orthogonal frequency division multiplexing with index modulation," *IEEE Trans. Commun.*, vol. 65, no. 9, pp. 3892–3906, Sep. 2017.
[14] E. Ozturk, E. Başar, and H. A. Cirpan, "Generalized frequency division multiplexing with index modulation," in *Proc. IEEE Globecom Workshops (GC Wkshps)*, Washington, DC, USA, Dec. 2016, pp. 1–6.
[15] E. Öztürk, E. Başar, and H. A. Çırpan, "Generalized frequency division multiplexing with flexible index modulation," *IEEE Access*, Oct. 2017.
[16] E. Başar, "Multiple-input multiple-output OFDM with index modulation," *IEEE Signal Process. Lett.*, vol. 22, no. 12, pp. 2259–2263, Dec. 2015.
[17] E. Başar, "On multiple-input multiple-output OFDM with index modulation for next generation wireless networks," *IEEE Trans. Signal Process.*, vol. 64, no. 15, pp. 3868–3878, Aug. 2016.
[18] L. Wang, Z. Chen, Z. Gong, and M. Wu, "Space-frequency coded index modulation with linear-complexity maximum likelihood receiver in the MIMO-OFDM system," *IEEE Signal Process. Lett.*, vol. 23, no. 10, pp. 1439–1443, Oct. 2016.
[19] B. Zheng, M. Wen, E. Başar, and F. Chen, "Multiple-input multiple-output OFDM with index modulation: Low-complexity detector design," *IEEE Trans. Signal Process.*, vol. 65, no. 11, pp. 2758–2772, Jun. 2017.
[20] M. Wen, X. Cheng, and L. Yang, "Optimizing the energy efficiency of OFDM with index modulation," in *Proc. IEEE Int. Conf. Commun. Syst.*, Macau, China, Nov. 2014, pp. 31–35.
[21] Y. Xiao, S. Wang, L. Dan, X. Lei, P. Yang, and W. Xiang, "OFDM with interleaved subcarrier-index modulation," *IEEE Commun. Lett.*, vol. 18, no. 8, pp. 1447–1450, Aug. 2014.
[22] M. Wen, M. Zhang, J. Li, E. Basar, and F. Chen, "Equiprobable subcarrier activation method for OFDM with index modulation," *IEEE Commun. Lett.*, vol. 20, no. 12, pp. 2386–2389, Dec. 2016.
[23] X. Yang, Z. Zhang, P. Fu, and J. Zhang, "Spectrum-efficient index modulation with improved constellation mapping," in *Proc. Int. Workshop High Mobility Wireless Commun. (HMWC)*, Xi'an, China, Oct. 2015, pp. 91–95.

[24] R. Fan, Y. J. Yu, and Y. L. Guan, "Generalization of orthogonal frequency division multiplexing with index modulation," *IEEE Trans. Wireless Commun.*, vol. 14, no. 10, pp. 5350–5359, Oct. 2015.
[25] R. Fan, Y. J. Yu, and Y. L. Guan, "Improved orthogonal frequency division multiplexing with generalised index modulation," *IET Commun.*, vol. 10, no. 8, pp. 969–974, May 2016.
[26] Q. Ma, Y. Xiao, L. Dan, P. Yang, L. Peng, and S. Li, "Subcarrier allocation for OFDM with index modulation," *IEEE Commun. Lett.*, vol. 20, no. 7, pp. 1469–1472, Jul. 2016.
[27] N. Ishikawa, S. Sugiura, and L. Hanzo, "Subcarrier-index modulation aided OFDM—Will it work?" *IEEE Access*, vol. 4, pp. 2580–2593, 2016.
[28] Y. Liu, M. Zhang, H. Wang, and X. Cheng, "Spatial modulation orthogonal frequency division multiplexing with subcarrier index modulation for V2X communications," in *Proc. Int. Conf. Comput., Netw. Commun. (ICNC)*, Kauai, HI, USA, Feb. 2016, pp. 1–5.
[29] X. Zhou, X. Cheng, and L. Yang, "Quadrature index modulated OFDM for vehicular communications," in *Proc. Int. Conf. Comput., Netw. Commun. (ICNC)*, Kauai, HI, USA, Feb. 2016, pp. 1–5.
[30] Y. Li, M. Wen, X. Cheng, and L.-Q. Yang, "Index modulated OFDM with ICI self-cancellation for V2X communications," in *Proc. Int. Conf. Comput., Netw. Commun. (ICNC)*, Kauai, HI, USA, Feb. 2016, pp. 1–5.
[31] S. A. Altalib, B. M. Ali, and A. I. Siddiq, "BER performance improvement of V2I communication by using OFDM IM exploiting all subcarrier activation patternser," in *Proc. Int. Conf. Commun., Control, Comput. Electron. Eng. (ICCCCEE)*, Khartoum, Sudan, Jan. 2017, pp. 1–4.
[32] M. Wen, Y. Li, X. Cheng, and L. Yang, "Index modulated OFDM with ICI self-cancellation in underwater acoustic communications," in *Proc. IEEE Asilomar Conf. Signals, Syst. Comput.*, Pacific Grove, CA, USA, Nov. 2014, pp. 338–342.
[33] L. Xiao, B. Xu, H. Bai, Y. Xiao, X. Lei, and S. Li, "Performance evaluation in PAPR and ICI for ISIM-OFDM systems," in *Proc. Int. Workshop High Mobility Wireless Commun.*, Beijing, China, Nov. 2014, pp. 84–88.
[34] Y. Li, M. Zhang, X. Cheng, M. Wen, and L.-Q. Yang, "Index modulated OFDM with intercarrier interference cancellation," in *Proc. IEEE Int. Conf. Commun. (ICC)*, Kuala Lumpur, Malaysia, May 2016, pp. 1–6.
[35] Q. Ma, P. Yang, Y. Xiao, H. Bai, and S. Li, "Error probability analysis of OFDM-IM with carrier frequency offset," *IEEE Commun. Lett.*, vol. 20, no. 12, pp. 2434–2437, Dec. 2016.
[36] S. Coleri, M. Ergen, A. Puri, and A. Bahai, "Channel estimation techniques based on pilot arrangement in OFDM systems," *IEEE Trans. Broadcast.*, vol. 48, no. 3, pp. 223–229, Sep. 2002.
[37] J.-J. van de Beek, M. Sandell, and P. O. Borjesson, "ML estimation of time and frequency offset in OFDM systems," *IEEE Trans. Signal Process.*, vol. 45, no. 7, pp. 1800–1805, Jul. 1997.
[38] X. Dong, W. S. Lu, and A. C. K. Soong, "Linear interpolation in pilot symbol assisted channel estimation for OFDM," *IEEE Trans. Wireless Commun.*, vol. 6, no. 5, pp. 1910–1920, May 2007.
[39] National Instruments. (2017). *NI-USRP 14.0—Windows—A Newer Version is Available*. Accessed: Jul. 6, 2017. [Online]. Available: http://www.ni.com/download/ni-usrp-14.0/4999/en/
[40] H. Arslan and S. Reddy, "Noise power and SNR estimation for OFDM based wireless communication systems," in *Proc. 3rd IASTED Int. Conf. Wireless Opt. Commun. (WOC)*, Banff, AB, Canada, Jan. 2003, pp. 1–6.

SELAHATTIN GOKCELI (S'17) received the B.S. and M.S. degrees in electronics and communication engineering from Istanbul Technical University, Istanbul, Turkey in 2015 and 2017, respectively, where he is currently pursuing the Ph.D. degree in telecommunication engineering. He has been serving as a member of the ITU Wireless Communication Research Laboratory since 2014. He is also an NI Certified LabVIEW Associate Developer. He has used LabVIEW as a programming tool in projects, such as software defined radio implementations of OFDMA-based NCC systems, cooperative communication, and 5G techniques like full-duplex communication. His research interests include cooperative communication network, physical layer security, and 5G waveform design.

ERTUGRUL BASAR (S'09–M'13–SM'16) received the B.S. degree (Hons.) from Istanbul University, Turkey, in 2007, and the M.S. and Ph.D. degrees from Istanbul Technical University in 2009 and 2013, respectively. From 2011 to 2012, he was with the Department of Electrical Engineering, Princeton University, NJ, USA. He was an Assistant Professor with Istanbul Technical University from 2014 to 2017, where he is currently an Associate Professor of electronics and communication engineering. He is an inventor of two pending patents on index modulation schemes. His primary research interests include MIMO systems, index modulation, cooperative communications, OFDM, and visible light communications.

Dr. Basar was a recipient of the Istanbul Technical University Best Ph.D. Thesis Award in 2014 and has received three best paper awards, including one from the IEEE International Conference on Communications 2016. He is a regular reviewer for various IEEE journals and has served as a TPC member for several conferences. He currently serves as an Associate Editor for the IEEE COMMUNICATIONS LETTERS and the IEEE ACCESS, and an Editor for the *Physical Communication* (Elsevier).

MIAOWEN WEN (M'14) received the B.S. degree from Beijing Jiaotong University, Beijing, China, in 2009, and the Ph.D. degree from Peking University, Beijing, China, in 2014. From 2012 to 2013, he was a Visiting Student Research Collaborator with Princeton University, Princeton, NJ, USA. He is currently an Associate Professor with the South China University of Technology, Guangzhou, China. He has authored a book and over 70 papers in refereed journals and conference proceedings. His research interests include index modulation and nonorthogonal multiple access techniques.

Dr. Wen received the Best Paper Award from the IEEE International Conference on Intelligent Transportation Systems Telecommunications in 2012, the IEEE International Conference on Intelligent Transportation Systems in 2014, and the IEEE International Conference on Computing, Networking and Communications in 2016. He received the Excellent Doctoral Dissertation Award from Peking University. He currently serves as an Associate Editor for the IEEE ACCESS, and on the Editorial Board of the *EURASIP Journal on Wireless Communications and Networking* and the ETRI journal.

Gunes Karabulut Kurt (M'06–SM'15) received the B.S. degree (Hons.) in electronics and electrical engineering from Bogazici University, Istanbul, Turkey, in 2000, and the M.A.Sc. and Ph.D. degrees in electrical engineering from the University of Ottawa, ON, Canada, in 2002 and 2006, respectively. From 2000 to 2005, she was a Research Assistant with the CASP Group, University of Ottawa. From 2005 to 2006, she was with TenXc Wireless, where she was involved in location estimation and radio-frequency identification systems. From 2006 to 2008, she was with Edgewater Computer Systems Inc., where she was involved in high-bandwidth networking in aircraft and priority based signaling methodologies. From 2008 to 2010, she was with Turkcell Research and Development Applied Research and Technology, Istanbul. Since 2010, she has been with Istanbul Technical University. Her research interests include sparse signal decomposition algorithms, multicarrier networks, traffic analysis, and network planning/management. She is a Marie Curie Fellow.